JOURNAL OF MATERIALS SCIENCE 37 (2002) 709–716

Influence of heat treatment on fatigue crack growth of austempered ductile iron

CHIH-KUANG LIN*, CHIH-WEI CHANG
Department of Mechanical Engineering, National Central University, Chung-Li 32054, Taiwan, ROC
E-mail: t330014@cc.ncu.edu.tw

Fatigue crack growth (FCG) behavior has been investigated for two different grades of austempered ductile irons (ADIs). These ADIs were produced from an alloyed ductile iron (DI) and heat treated respectively at two austempering temperatures, 300 and 360°C, to generate two different ausferrite microstructures. FCG tests using compact tension (CT) specimens were conducted under load control with three load ratios, $R = 0.1$, 0.5 and 0.7. The fatigue crack growth rates (FCGRs) of the given ADIs were compared with those of the as-cast DI with a bull's eye microstructure to examine the influence of austempering treatment on the FCG behavior of DI. The FCG behavior for the given materials was found to be dependent on the matrix structure with a demonstration that the as-cast DI had a better FCG resistance than did the ADIs at low ΔK regime and vice versa at high ΔK regime. As for the comparison made between the two ADIs, the one austempered at 360°C exhibited a lower FCG rate as a result of its coarse ausferrite microstructure, higher volume fraction of retained austenite, and greater toughness. The ADIs also demonstrated a load ratio dependence of intrinsic FCGR; that is, the enhancement of the FCGR with an increase in R value could not be rationalized by the crack closure effects.

1. Introduction

Austempered ductile irons (ADIs) have been recently developed for an increasing number of engineering applications such as gears, crankshafts, connecting rods and others in heavy machinery and transportation equipment because they offer excellent combinations of high strength, ductility, toughness, fatigue strength, and wear resistance over other grades of cast irons [1–3]. Different combinations of these mechanical properties can be tailored to suit particular applications by proper adjustment of alloy elements and austempering treatments. The unique microstructure possessed by ADIs consists of acicular, carbide-free ferrite with carbon-enriched austenite. This microstructure has been called "ausferrite" to distinguish it from the bainite structure in steels [4]. The desirable mechanical properties of ADI are comparable, or in some cases superior to those of forged steel. Low cost and design flexibility are additional advantages of ADIs over forgings for applications in transportation industry [1–3].

High-cycle fatigue (HCF) properties of ADI have been studied extensively [5–16] by generating the stress-life (S-N) curves under various base-iron compositions and heat treatments. It has been reported that the fatigue limit of ADI is not proportional to tensile strength or hardness [6, 7, 10–12, 14–16] as with most steels. In general, ADI with a larger volume fraction of retained austenite and greater toughness has a better HCF performance and higher fatigue limit [1, 5–7, 11–16]. It is believed that the retained austenite ahead of the fatigue crack tip may transform to martensite under deformation leading to crack growth retardation [7, 14, 15]. However, it has been reported by Lin *et al*. [14, 15, 17, 18] that the influence of ausferritic structure on the HCF and strain-controlled low-cycle fatigue (LCF) behavior of ADI was different. ADI with a larger volume fraction of retained austenite showed better HCF resistance but inferior LCF performance [14, 15, 17, 18]. This is related to the stability of retained austenite and the associated fatigue loading modes and magnitudes during test [14, 15, 17, 18]. As for the influence of retained austenite content and ausferritic microstructure on the fatigue crack growth (FCG) behavior of long crack in ADI, there is still lack of consistent conclusions due to limited number of studies in this area. For example, it has been reported that a coarse ausferritic matrix structure with a higher volume fraction of retained austenite in ADI austempered at temperatures ranging from 350 to 400°C, would provide better FCG resistance in comparison to that austempered at a lower temperature [11, 19, 20]. However, another study [21] indicated that the fatigue crack growth rate (FCGR) of long crack in ADI was rarely affected by the difference in the ausferritic

*Author to whom all correspondence should be addressed.

matrix structures generated at two austempering temperatures, 260 and 360°C. Apparently, more research is needed to characterize the effects of austempering treatment and, in particular, the associated ausferritic matrix structure and retained austenite on the FCG behavior of ADI in long-crack regime.

As the applications of ADI in engineering components involve using castings of various geometries subjected to long-term mechanical, variable loads, it is important to understand the fatigue behavior and develop a useful lifetime prediction methodology for this advanced cast iron under various loading and cracking conditions. The fundamental fatigue damage processes, such as HCF and LCF, of ADI have been studied extensively by the first author and co-workers [14–18, 22]. As part of a series of studies on the fatigue strength assessment of ADI, the current work is to characterize the effects of austempering treatment and associated microstructure on the long-crack FCG behavior of ADI by conducting systematic FCG experiments at different load ratios on selected ductile irons (DIs) in as-cast and two differently austempered conditions.

2. Materials and experimental procedures

The material used in the current study is an alloyed DI with a chemical composition (wt%): 3.53 C, 2.27 Si, 0.47 Ni, 0.43 Cu, 0.22 Mn, 0.17 Mo, 0.04 Mg, 0.026 P, 0.009 S, and balance of Fe. The DI was cast into a standard Y-block form at a local high-production commercial foundry using sand molds. The riser of each Y-block casting was first cut off and the remaining leg section in 25 mm thickness was used to make specimens for metallography, tensile and FCG testing. The graphite structure in selected casting portions has the following measured data: average nodule diameter of 34 μm, nodularity of ~90%, and nodule counts of ~90 nodules/mm^2. The tensile properties were obtained by using tensile specimens having a cylindrical gage section of 6 mm in diameter and 25 mm in length. FCG experiments were performed in accordance with ASTM E647 on 6.35-mm-thick compact tension (CT) specimens (Fig. 1) to determine the da/dN-ΔK relationship.

Two different austempering treatments were applied to investigate the influence of different ausferritic structures on the FCG behavior. Test specimens were first austenitized in salt bath at 900°C for 1.5 h after which they were quenched in salt bath either at 300°C, 3 h for a higher strength (designated as ADI I) or at 360°C, 2 h for a greater toughness (designated as ADI II); they were then cooled in forced air. Detailed description in selecting these two austempering conditions for the DIs with similar chemical compositions are given elsewhere [14]. Mechanical properties in these two austempered and the as-cast conditions are given in Table I which indicates the austempering treatment indeed improves the strength and hardness of the DI. In addition, the ultimate tensile strength, yield strength, and hardness obtained at 300°C are respectively greater than those obtained at 360°C while the elongation and toughness take the reverse trend. As reported previously [14], these differences in mechanical properties can be attributed to the variation of matrix structure as shown in Fig. 2. The microstructure of the as-cast DI consists of a bull's eye ferrite structure in pearlitic matrix (Fig. 2a) which is different from the ausferritic ones in ADI I and II. Note that a change from a fine (Fig. 2b) to coarse (Fig. 2c) ausferritic matrix structure can be seen as the austempering temperature increases. The greater toughness and ductility obtained at 360°C result from a greater amount of retained austenite present in the matrix (Fig. 2c). X-ray diffraction analysis results show the average volume fraction of retained austenite, before any mechanical testing, for ADI II is significantly greater than that for ADI I; i.e., 30.3% versus 15.9%.

TABLE I Mechanical properties of various ductile irons tested

Type	Tensile strength (MPa)	Yield strength (MPa)	Modulus of elasticity (GPa)	Elongation (in 25 mm) (%)	Impact energy (J)	Hardness (HRc)
As-cast	772	448	160	7.09	36.5	21.8
ADI-I	1,333	1,320	171	0.20	70.1	50.5
ADI-II	1,036	901	167	1.64	143.0	38.0

FCG tests were conducted on a closed-loop, servohydraulic machine under a sinusoidal loading wave form with a frequency of $f = 20$ Hz and various load ratios, namely R (minimum load/maximum load) = 0.1, 0.5, and 0.7. Before any FCG testing, all CT specimens were

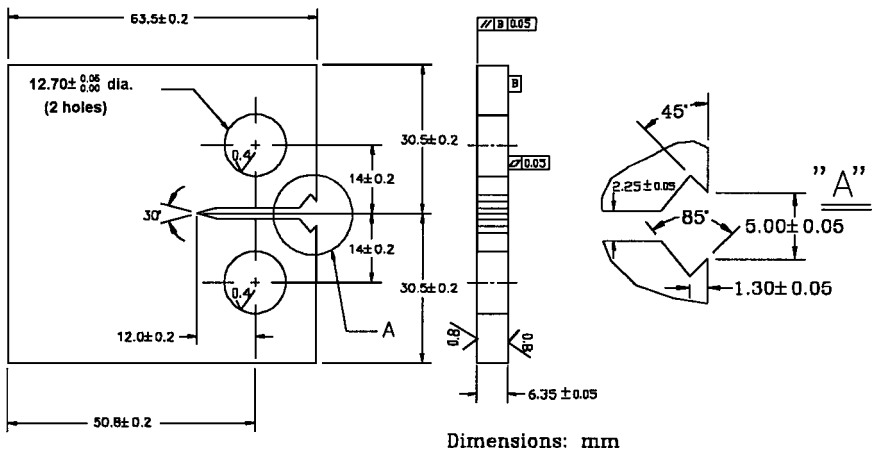

Figure 1 Geometry of compact tension specimen used in FCG test.

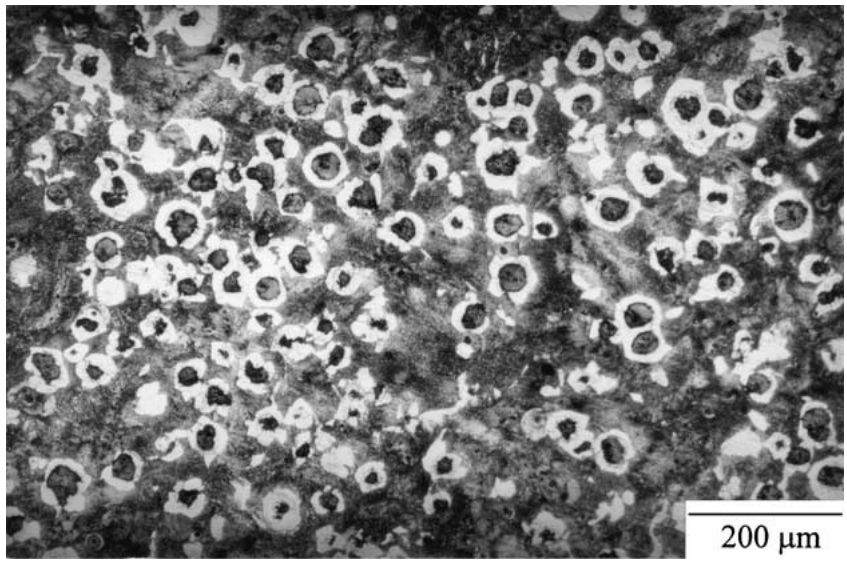

(a)

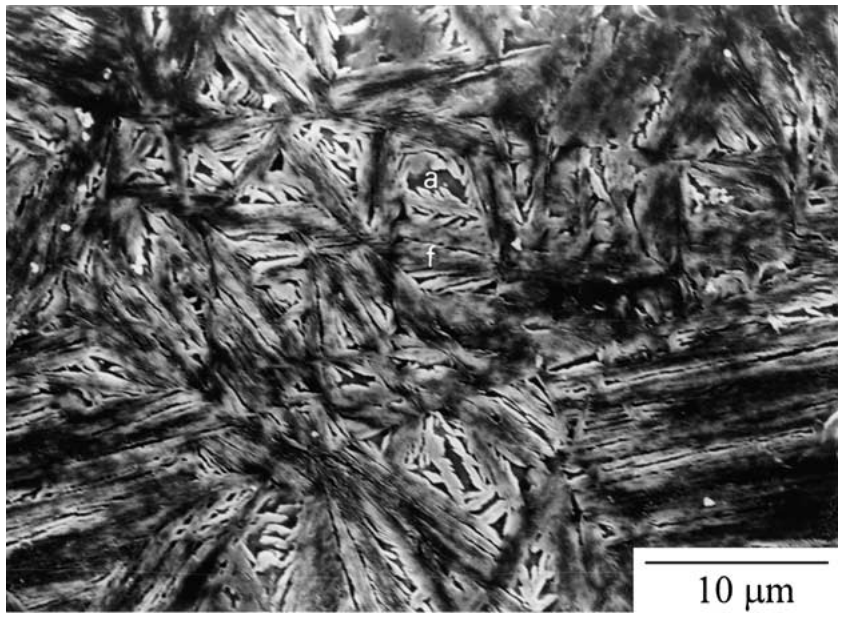

(b)

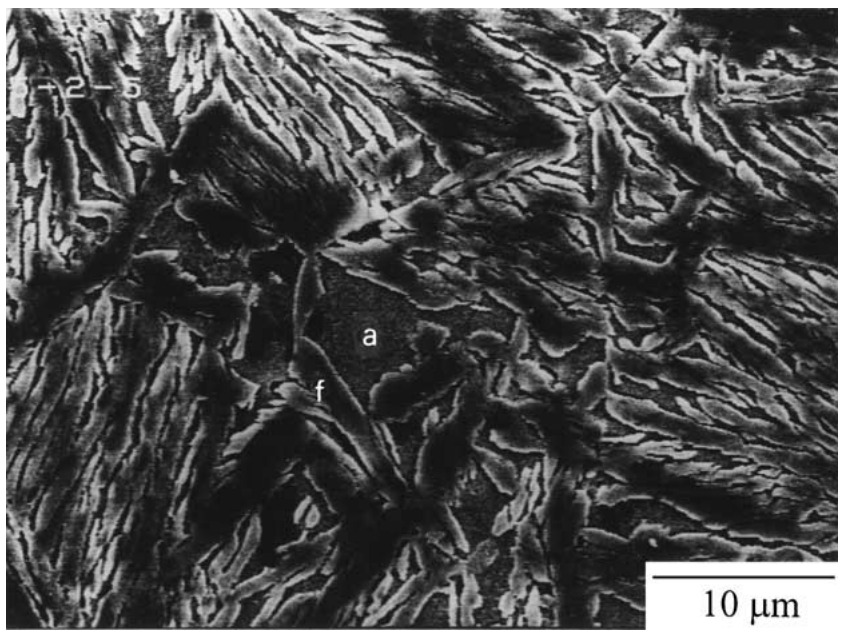

(c)

Figure 2 Typical matrix microstructures: (a) as-cast DI, (b) ADI-I, and (c) ADI-II (f: ferrite; a: austenite).

first fatigue precracked under $f = 20$ Hz and $R = 0.1$ to satisfy the requirements of ASTM E647 Standard. The crack length and crack closure level in the FCG tests were determined by the compliance technique recommended by ASTM E647 Standard using a clip gage mounted on the front edge of the CT specimen to monitor the crack-mouth-opening displacement during testing. Characterizations of the fracture surface morphology were made by scanning electron microscopy (SEM).

3. Results and discussion

3.1. Influence of microstructure on the fatigue crack growth rate

The FCGR data in the as-cast as well as two different austempered conditions were plotted as $(\mathrm{d}a/\mathrm{d}N)$ vs. (ΔK) in Fig. 3 under three various load ratios ($R = 0.1$, 0.5, and 0.7). The FCG behavior clearly shows a microstructural dependence as intersections of the FCGR curves for the as-cast DI and two ADIs occurred at certain transition ΔK values as shown in Fig. 3. For a given load ratio, the as-cast DI with a bull's eye matrix structure exhibited the lowest FCGR in the low ΔK regime and, presumably, a higher threshold stress intensity range, ΔK_{th}. In the high ΔK region, the ADIs with ausferritic matrix structures provided more or comparable FCG resistance as compared to the as-cast bull's eye microstructure depending on the R value. In addition, ADI II with a coarser ausferrite matrix structure and greater amount of retained austenite essentially exhibited lower FCGRs for the entire ΔK regime observed at $R = 0.1$ (Fig. 3a) than did ADI I with a finer ausferritic microstructure and lower volume fraction of retained austenite. The crack closure level (K_{op} value) was monitored throughout each FCG test to evaluate whether the observed microstructural dependence of the FCG behavior was due to crack closure effect or not. After factoring out the crack closure level, the FCGR results presented as a function of the effective stress intensity range, ΔK_{eff}, still indicated similar trends to those shown in Fig. 3. Therefore, the FCG resistance is not only different from bull's eye to ausferrite matrix structure but also different between fine and coarse ausferritic microstructures.

Consistent variations of the FCG behavior between the as-cast and variously austempered DIs were reported in an earlier study [19] in which the FCG resistance of the bull's eye microstructure was between that of the coarse and fine ausferrite microstructures. However, other studies [21, 23] showed that no microstructural effect on the FCG behavior could be seen, as the intrinsic FCGRs among the bull's eye, ferrite, pearlite and different ausferrite structures were not significantly different after subtracting the crack closure effect. Although the study by Greno *et al*. [21] indicated insensitivity of the FCGR in Region II (Paris-equation regime) to the microstructural effect for variously heat treated ADIs, it still reported a microstructural dependence of FCG behavior in the near threshold regime where an ADI austempered at 360°C exhibited greater values of fatigue threshold range, ΔK_{th}, at $R = 0.1$ than did the

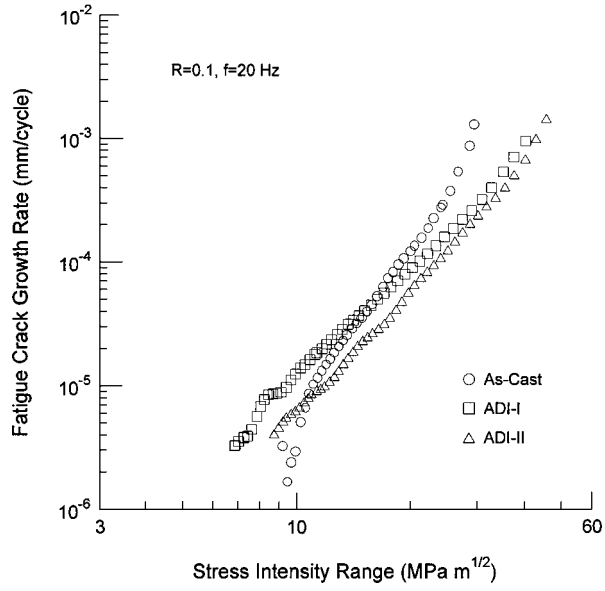

(a)

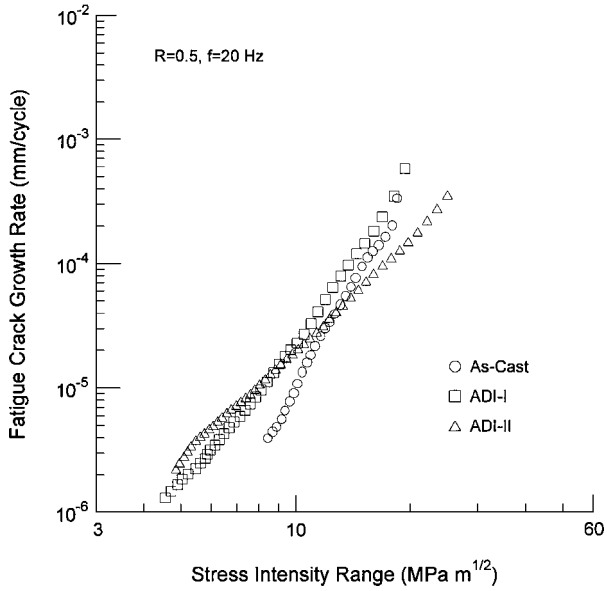

(b)

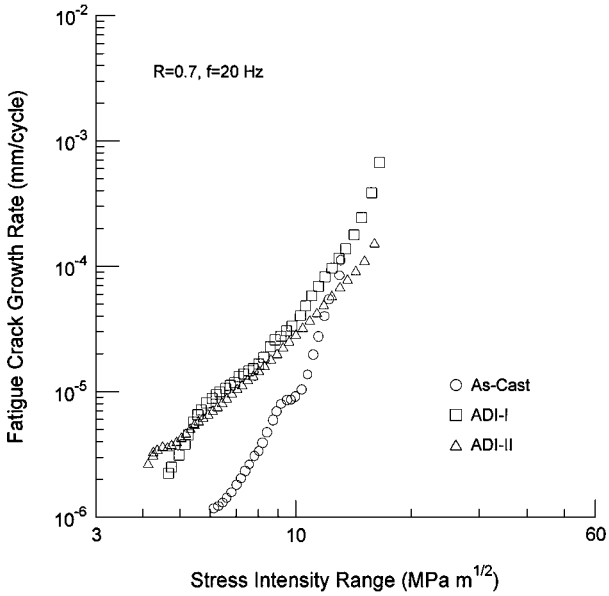

(c)

Figure 3 Comparison of fatigue crack growth rate curves for as-cast and austempered ductile irons at various load ratios: (a) $R = 0.1$, (b) $R = 0.5$ and (c) $R = 0.7$.

one austempered at 290°C. This is consistent with the trend between ADI I and ADI II shown in Fig. 3a and is attributed to the difference in the ausferritic structure as discussed below.

The graphite nodules, due to their low elastic moduli, are readily debonded from the matrix when cast iron is subjected to certain tensile loads. The stress concentration around the debonded graphite nodules would assist the nucleation and growth of microcracks from the nodule voids. In the low ΔK region, where the applied load levels are small, the driving force for the direct extension of the main crack is small such that the processes of linkage of microcracks emanating from the debonded-nodule voids and their coalescence with the main crack become the dominant stage in determining the FCGR. Therefore, the greater FCG resistance observed at low ΔK regime for the as-cast DI may be attributed to its greater resistance to extension and linkage of microcracks from the voids around the debonded graphite nodules. As the ferrite ring around a graphite nodule in a bull's eye matrix structure is more ductile than the ausferrite, it would be easier for the microcrack to nucleate from the nodule void in an ausferritic matrix than in a bull's eye structure. Therefore, there would be more microcracks to link with each other and readily coalesce with the main crack in the ADIs at low ΔK regime when the driving force for the growth of main crack is low. This might explain why the FCGRs were higher in the ADIs than in the as-cast DI at low ΔK regime. Evidences for this postulation are supported by the fractography observations. Fig. 4 shows the typical fractography observed at low ΔK regime for both as-cast and austempered DIs. It can be seen in Fig. 4b the microcracks emanating from the graphite nodules grew to link with each other by cutting through the debonded-nodule voids for the ADI. However, in Fig. 4a only microcracks surrounding the nodule voids were observed and no evidence of microcrack linkage was detected for the as-cast DI.

In the high ΔK region where the driving force for extension of the main crack became stronger, the main crack would be prompt to interact with the graphite nodules ahead of the crack tip. Therefore, the FCG behavior at high ΔK regime would be influenced mostly by the resistance of the matrix structure to the propagation of the main crack, i.e., the fracture toughness. As the ausferritic matrix structure in ADI provided more fracture toughness (Table I) than did the bull's eye microstructure, the FCGRs at higher ΔK values would be lower in ADIs than in as-cast DI. In particular, ADI II having a coarser ausferrite microstructure and greater fracture toughness essentially exhibited the slowest FCGR at the intermediate and high ΔK regions. It is believed that transformation of the unstable retained austenite under deformation to martensite around the highly stressed crack-tip area may also retard the growth of the main crack [7, 14, 15]. This deformation-induced martensitic transformation would relax the stress concentration at the crack tip and the accompanying volume change would also urge plastically induced crack closure to occur [7]. In this regard, ADI II with a greater volume fraction of retained austenite would obtain more beneficial effects from this deformation-induced martensitic transformation to reduce the FCGR of the main crack as compared to the as-cast DI and ADI I in high ΔK regime.

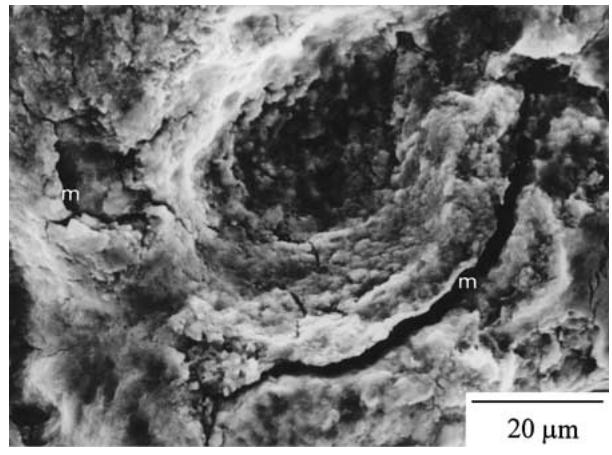

(a)

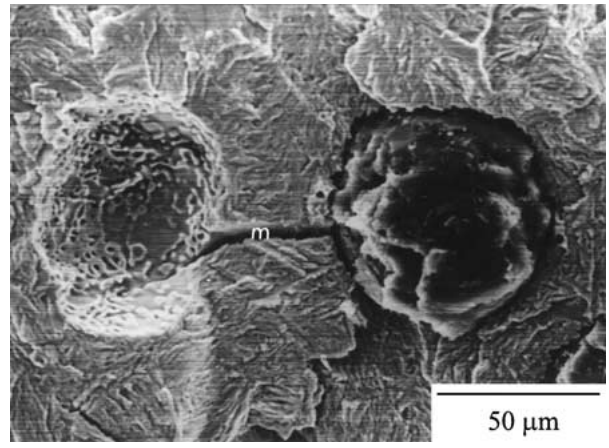

(b)

Figure 4 SEM fractography at low ΔK region for (a) as-cast and (b) austempered ductile irons (m: microcracks).

The micrograph in Fig. 5a shows the existence of martensite laths (label M) within a blocky retained austenite (label a) at a location very close to the path of the main crack on an ADI II specimen after FCG testing. However, as shown in Fig. 5b, no such morphology of martensite laths within the blocky retained austenite was observed at a region far away from the path of the main crack in the same ADI II specimen. X-ray diffraction analyses provided additional quantitative data showing a similar trend. The average volume fraction of the retained austenite along the crack path on the post-fracture ADI II CT specimen was found to be 24.7% which is lower than the value of 30.3% in the area far away from the crack path. The decrease in the amount of retained austenite along the crack path area implied some of the unstable retained austenite around the crack tip area had been transformed to martensite during the propagation of the main crack. As the retained austenite content in ADI I is considerably lower than that in ADI II (15.9% vs. 30.3%), the crack growth retardation effect induced by the martensitic transformation of unstable retained austenite at crack tip would be less effective in ADI I. However, the crack closure effect caused by this type of martensitic transformation

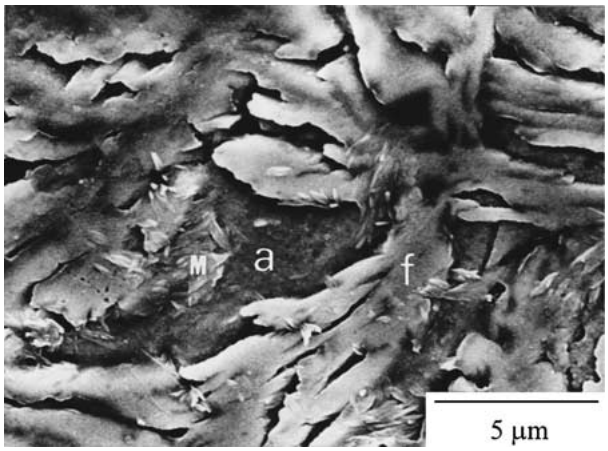

(a)

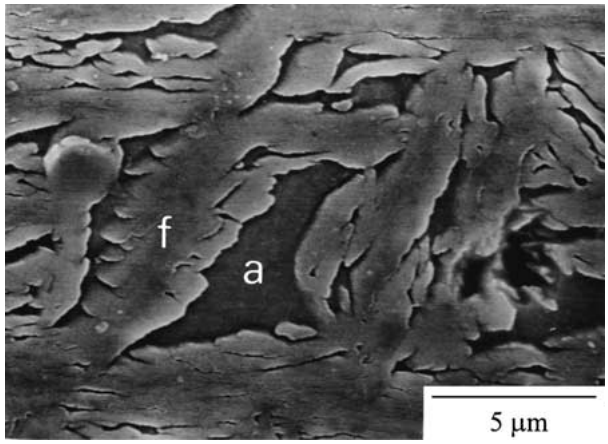

(b)

Figure 5 Microstructures of blocky retained austenite in ADI II at two different areas: (a) near the main crack path and (b) far away from the main crack (f: ferrite; a: austenite; M: martensite).

became insignificant when the load ratio was increased from 0.1 to 0.5 and 0.7 where K_{min} was always greater than K_{op}. This might explain why the FCGR differences between ADI I and ADI II became smaller at higher R values.

3.2. Influence of load ratio on the fatigue crack growth rate

Fig. 6 shows the comparison of FCGR at various load ratios for each material investigated. It can be seen in Fig. 6 that the FCGR was increased with an increase in load ratio for each material. The load ratio effects on the FCG behavior were more pronounced in the ADIs (Fig. 6b and c) than in the as-cast DI (Fig. 6a). In order to examine whether the influence of the load ratio on the FCGR was only due to the crack closure effect, the results presented in Fig. 6 were replotted in Fig. 7 as (da/dN) vs. ΔK_{eff} by taking into account the crack closure data. Here, $\Delta K_{eff} = (K_{max} - K_{op})$ if $K_{op} > K_{min}$, or $\Delta K_{eff} = \Delta K = (K_{max} - K_{min})$ if $K_{min} > K_{op}$. As shown in Fig. 7a, the influence of the load ratio on the FCGR became negligible at low ΔK_{eff} regime for the as-cast DI. However, the load ratio effects on the intrinsic FCGR were still existent at high ΔK_{eff} regime for the as-cast DI and in the entire ΔK_{eff} region for the two ADIs. In this regard, the mean stress effects on the FCG behavior could not be simply rationalized by the crack closure effect and might be related to certain

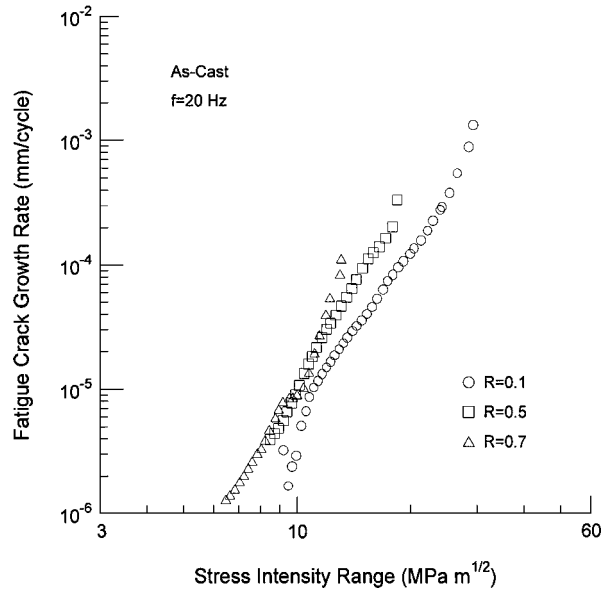

(a)

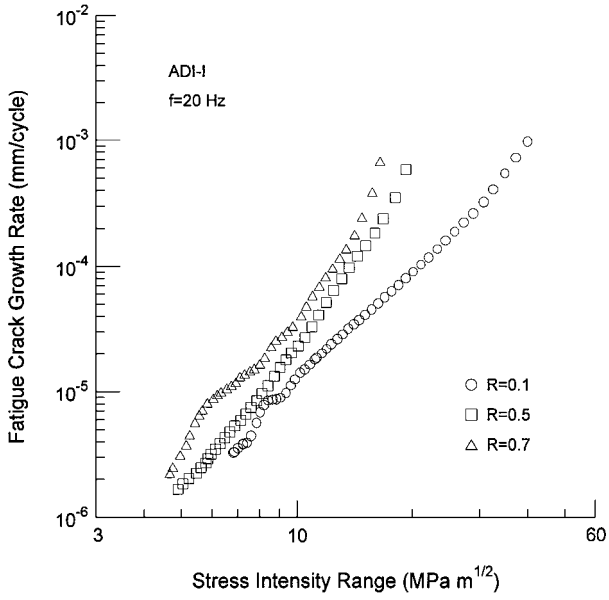

(b)

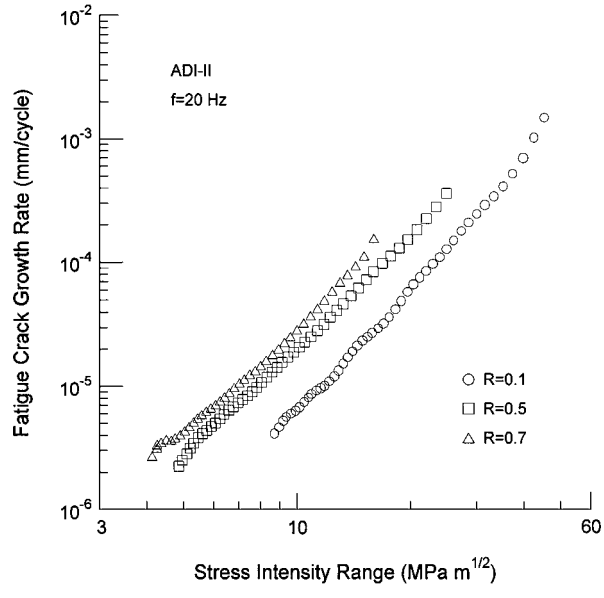

(c)

Figure 6 Comparison of fatigue crack growth rate curves at different load ratios in three given materials: (a) as-cast DI, (b) ADI I and (c) ADI II.

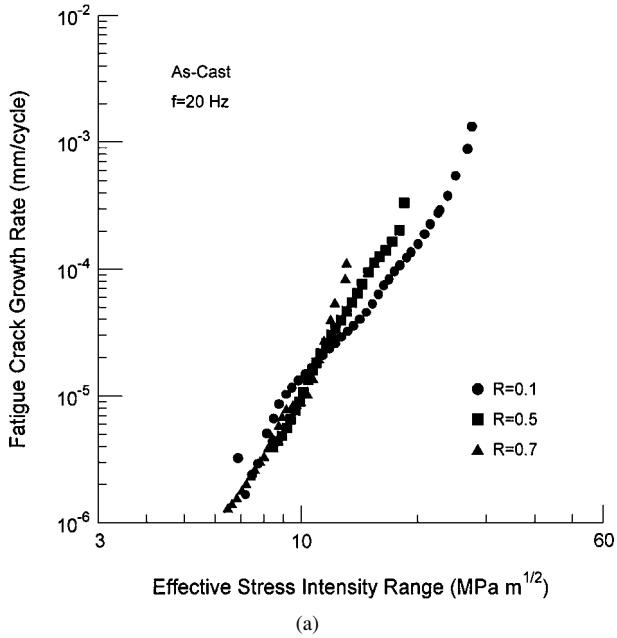

(a)

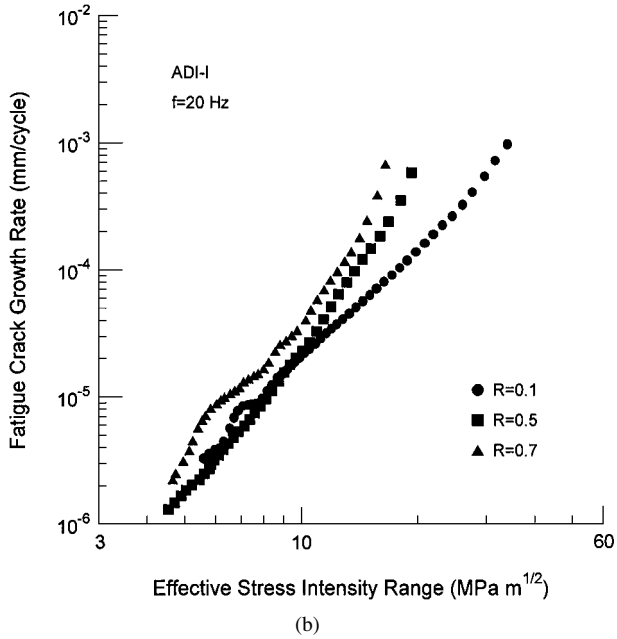

(b)

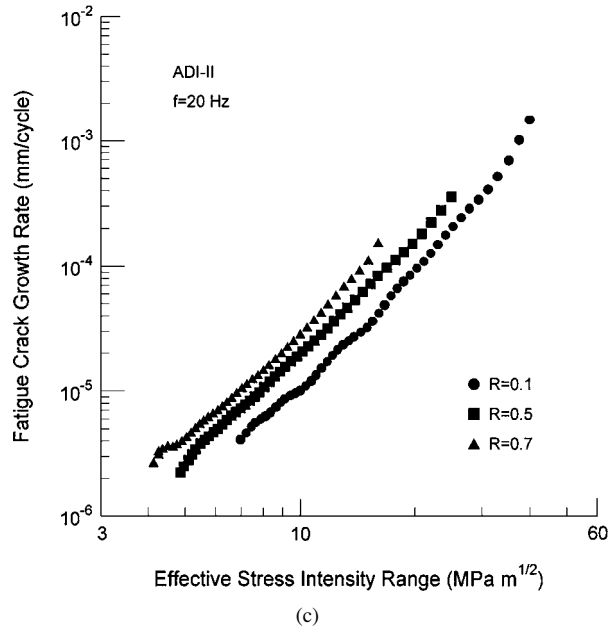

(c)

Figure 7 Comparison of (da/dN)-ΔK_{eff} curves at different load ratios in three given materials: (a) as-cast DI, (b) ADI I and (c) ADI II.

static fracture mechanisms. It has been reported in literature [10, 17, 18, 24–26] that the typical crack propagation path in various grades of DIs, including ADI, depends strongly on the location of the next graphite module ahead of the crack tip, and the crack front appears to connect the nodules along its path. Therefore, a static fracture mechanism related to the decohesion of graphite nodules ahead of the main crack tip is proposed to account for the true load ratio effects observed in the current study.

It can be seen in Fig. 7a that at $\Delta K_{\text{eff}} < 12$ MPa m$^{1/2}$ the intrinsic FCGRs were not considerably affected by the load ratio while a true mean stress effect became effective at $\Delta K_{\text{eff}} > 12$ MPa m$^{1/2}$ for the as-cast DI. In the low ΔK_{eff} region where the driving force for the growth of the main crack was less intensive, the highly stressed area ahead of the crack tip was small and the nominal stress level at the ligament region in the CT specimen was low. As a result, a smaller number of graphite nodules were debonded from the matrix due to a lower tensile static stress level was provided to break the interface bond. In addition, since the growth and linkage rather than the initiation of microcracks from the debonded-nodule voids played an important role in determining the growth rate of the main crack at low ΔK regime, the load ratio effects became insignificant in the bull's eye structure which had more resistance to growth of microcrack than the ausferrite. Accordingly, a high load ratio which would produce more debonded-nodule voids might not significantly affect the FCGR of the main crack at low ΔK regime in the as-cast DI. On the other hand, at the higher ΔK region, the main crack was provided with more driving force in promptly propagating toward the nodule-base microcracks or voids along its path. The more microcracks or debonded-nodule voids are accessible along the propagation path of the main crack, the greater enhancement in the FCGR of the main crack will occur. Consequently, an increase in the load ratio would increase the static stress level and generate more debonded-nodule voids leading to an increase in the FCGR at high ΔK regime for the as-cast DI.

Fig. 7b and c showed the intrinsic FCGR for both ADIs was enhanced with an increase in load ratio at all of the testing ΔK_{eff} region indicating the existence of true load ratio effects on FCG regardless of the intensity of the driving force for the extension of the main crack. As described above, the resistance to the microcrack growth from the debonded-nodule void was smaller in an ausferrite matrix than in a bull's eye structure resulting in more linking microcracks available to coalesce with the main crack in ADI than in as-cast DI even though in the low ΔK regime. Therefore, fatigue loading with a higher load ratio would provide more nucleation and extension of microcracks ahead of the crack tip in an ausferritic microstructure such that the intrinsic FCGR of the main crack was essentially increased in ADI with increasing R value.

4. Conclusions

1. In the low ΔK region, the FCGR was slower in the as-cast DI than in the ADIs due to the greater resistance

to growth of microcracks from debonded graphite nodule voids in the bull's eye matrix structure.

2. At high ΔK regime, ADIs having greater fracture toughness from the ausferrite structures exhibited more resistance to the extension of main crack and lower FCGRs than did the as-cast DI.

3. More FCG resistance was observed in ADI austempered at 360°C as a result of the greater toughness from its coarser ausferrite microstructure and larger amount of retained austenite, as compared to that austempered at 300°C. A greater volume fraction of retained austenite was likely to produce more beneficial effects from the martensitic transformation of retained austenite ahead of the crack tip to retard the crack growth.

4. The FCGR in ADI was found to be increased with increasing load ratio. A static fracture mechanism related to the decohesion of graphite nodules ahead of the main crack tip was proposed to account for the true load ratio effects on FCG behavior observed in the current study.

Acknowledgements

This work was funded by the National Science Council of the Republic of China (Taiwan) under Contract No. NSC-88-2216-E-008-006.

References

1. Y. TANAKA and H. KAGE, *Mater. Trans., JIM* **33** (1992) 543.
2. B. V. KOVACS, *J. Heat Treat.* **5** (1987) 55.
3. T. N. ROUNS, K. B. RUNDMAN and D. M. MOORE, *AFS Trans.* **92** (1984) 815.
4. B. V. KOVACS, *ibid.* **102** (1994) 417.
5. K. JOKIPII, in Proceedings of the First International Conference on ADI (American Society for Metals, 1984) p. 135.
6. S. YOSHINO, in Proceedings of the Second International Conference on ADI (ASME-Gear Research Institute, 1986) p. 337.
7. M. GRECH and J. M. YOUNG, *AFS Trans.* **98** (1990) 341.
8. G. P. FAUBERT, D. J. MOORE and K. B. RUNDMAN, *ibid.* **99** (1991) 563.
9. K. L. HAYRYNEN, D. J. MOORE and K. B. RUNDMAN, *ibid.* **100** (1992) 93.
10. K. P. JEN, J. WU and S. KIM, *ibid.* **100** (1992) 833.
11. L. BARTOSIEWICZ, A. R. KRAUSE, F. A. ALBERTS, I. SINGH and S. K. PUTATUNDA, *Materials Characterization* **30** (1993) 221.
12. P. SHANMUGAN, P. P. RAO, K. R. UDUDA and N. VENKATARAMAN, *J. Mater. Sci.* **29** (1994) 4933.
13. M. BAHMANI, R. ELLIOTT and N. VARAHRAM, *ibid.* **32** (1997) 5383.
14. C.-K. LIN, P.-K. LAI and T.-S. SHIH, *Int. J. Fatigue* **18** (1996) 297.
15. C.-K. LIN and J.-Y. WEI, *Mater. Trans., JIM* **38** (1997) 682.
16. C.-K. LIN and W.-J. LEE, *Int. J. Fatigue* **20** (1998) 301.
17. C.-K. LIN and T.-P. HUNG, *ibid.* **18** (1996) 309.
18. C.-K. LIN and C.-S. FU, *Mater. Trans., JIM* **38** (1997) 693.
19. J.-L. DOONG and S.-I. YU, *Int. J. Fatigue* **10** (1988) 219.
20. L. BARTOSIEWICZ, A. R. KRAUSE, B. KOVACS and S. K. PUTATUNDA, *AFS Trans.* **100** (1992) 135.
21. G. L. GRENO, J. L. OTEGUI and R. E. BOERI, *Int. J. Fatigue* **21** (1999) 35.
22. C.-K. LIN and Y.-L. PAI, *ibid.* **21** (1999) 45.
23. K. TOKAJI, T. OGAWA and K. SHAMOTO, *ibid.* **16** (1994) 344.
24. J. H. BULLOCH, *Thr. Appl. Fract. Mech.* **17** (1992) 19.
25. Z. K. FAN and R. E. SMALLMAN, *Scripta Metall. et Mater.* **31** (1994) 137.
26. B. J. WENG, S. T. CHUNG, H. N. LIU and S. E. HSU, *Chn. J. Mater. Sci.* **23** (1991) 278 (in Chinese).

Received 10 April
and accepted 9 October 2001